Research Square

Preprints are preliminary reports that have not undergone peer review.
They should not be considered conclusive, used to inform clinical practice,
or referenced by the media as validated information.

Toward Skin-Tone-Aware Hypoxia Detection: A Raspberry Pi System Fusing Pulse Oximetry and Fingertip Image Analysis

Rethwan Faiz

rethwan_faiz@aiub.edu

American International University-Bangladesh

Md. Rubayat Haque Nobo

American International University-Bangladesh

Mohammad Hasan Imam

American International University-Bangladesh

Dibas Dhar

American International University-Bangladesh

Zabin Tasmin

American International University-Bangladesh

Nuzat Nuary Alam

American International University-Bangladesh

Research Article

Keywords: Hypoxia detection, Pulse oximetry, Skin-tone bias, Convolutional neural network, SpO_2, Sensor fusion, Embedded biomedical system

Posted Date: November 26th, 2026

DOI: https://doi.org/10.21203/rs.3.rs-11682316/v1

License: This work is licensed under a Creative Commons Attribution 4.0 International License.
Read Full License

Additional Declarations: No competing interests reported.

ORIGINAL RESEARCH ARTICLE

Toward Skin-Tone-Aware Hypoxia Detection: A Raspberry Pi System Fusing Pulse Oximetry and Fingertip Image Analysis

Rethwan Faiz, Md. Rubayat Haque Nobo, Mohammad Hasan Imam, Dibas Dhar, Zabin Tasmin, Nuzat Nuary Alam
Department of Electrical and Electronic Engineering, American International University-Bangladesh, Dhaka, Bangladesh
** Corresponding author: rethwan_faiz@aiub.edu*

Author emails: rethwan.faiz@aiub.edu; 22-46214-1@student.aiub.edu; hasan.imam@aiub.edu; 22-46007-1@student.aiub.edu; 22-46218-1@student.aiub.edu; nuzatalam@aiub.edu;

Abstract

Background: Conventional pulse oximeters can overestimate arterial oxygen saturation (SpO_2) in patients with darker skin tones, particularly during hypoxemia. No low-cost embedded system currently combines contact-based pulse oximetry with complementary deep-learning image classification on a single embedded platform while explicitly targeting skin-tone-aware screening.

Methods: A Raspberry Pi 4 Model B coordinated a MAX30100 pulse-oximetry sensor and a Pi Camera Module to simultaneously acquire SpO_2 readings and 224×224-pixel fingertip images. A TensorFlow/Keras convolutional neural network (CNN) was trained with class-aware oversampling of presumed skin-tone-diverse and low-SpO_2 cases (standardized skin-tone labels were not collected, so pigmentation coverage cannot be quantified post hoc). CNN hypoxia probability and a logistic mapping of the contemporaneous SpO_2 reading (centred at 94%) were combined into a fused probability; hypoxia was reported when the fused value exceeded 0.5. Performance was assessed on a held-out validation set (N = 53) using Wilson 95% confidence intervals, Matthews correlation coefficient (MCC), and balanced accuracy.

Results: Overall accuracy was 83%, balanced accuracy 0.84, MCC 0.71, and AUC 0.97. Hypoxia recall was 1.00 (95% CI 0.87–1.00; 25/25 cases correctly identified); normal-class recall was 0.68 (95% CI 0.49–0.82). These estimates carry wide confidence intervals reflecting the small validation sample. Real-time hardware trials across four physiological states (SpO_2 87–97%) reproduced the offline classification output exactly in all four cases.

Conclusions: Sensor–vision fusion on a low-cost Raspberry Pi is technically feasible and achieved zero false negatives in this pilot, supporting its potential as a skin-tone-aware screening adjunct to conventional pulse oximetry. Substantially larger datasets with standardized skin-tone labelling and clinically supervised hypoxia induction are required before any clinical validity claim can be made.

Keywords: Hypoxia detection; Pulse oximetry; Skin-tone bias; Convolutional neural network; SpO_2; Sensor fusion; Embedded biomedical system

Background

Accurate measurement of arterial oxygen saturation (SpO_2) is critical for time-sensitive clinical decisions, yet conventional photoplethysmography (PPG)-based pulse oximeters frequently produce inaccurate readings due to skin pigmentation, ambient lighting, and the hypoxic state itself. Multiple independent clinical audits have documented that finger-based pulse oximeters systematically overestimate SpO_2 in patients with darker skin tones during hypoxemia, delaying recognition of a dangerous condition in the population least well served by the device [4].

Prior work has improved the underlying optical measurement — multi-wavelength PPG platforms [1], melanin-aware optical modelling [2], wavelength-selection optimization [3], camera- and video-based SpO_2 estimation [5],[6], and SpO_2-derived applications such as nocturnal hypoxemia and sleep-stage classification [7],[8]. The bias mechanism itself has been linked to signal-to-noise-ratio-dependent error in the R-value calculation that scales with melanin concentration [9], with related work on signal-quality control [10]–[13], multimodal sensing [14], reflectance modelling [15], and acquisition hardware [16]–[20]. Table 1 summarizes representative approaches. Despite this progress, no existing system combines a low-cost embedded acquisition platform, an image-based classifier trained explicitly for skin-tone sensitivity, and fusion with a contact sensor to provide a safety-oriented, high-recall second opinion; existing calibration corrections do not fully compensate for melanin-induced optical variability.

Table 1. Representative prior approaches to SpO_2 estimation and bias mitigation, compared with the present work.

Ref.	Approach	Reported outcome
[1]	Multi-wavelength PPG, 1 ksps	HR ±4.08 bpm, SpO_2 ±1.54%; adds hematocrit (RHCT) estimation
[2]	Monte Carlo melanin modelling	Melanin concentration significantly alters reflectance-based SpO_2 accuracy
[4]	Clinical bias audit	Darker skin tones show systematic SpO_2 overestimation under hypoxemia
[5]	Smartphone camera + CNN	Non-contact SpO_2 alternative to contact sensors
[6]	Wearable lens-integrated sensor	SpO_2 RMSE 2.61%, HR RMSE 1.6%
[9]	SNR-based bias analysis	Bias in R-value scales with melanin concentration
[14]	3D time-of-flight + SpO_2 fusion	ICC = 0.94 vs. manual scoring; 80% severity classification
This work	MAX30100 + CNN fingertip classifier, embedded Raspberry Pi	83% accuracy, AUC 0.97, hypoxia recall 1.00 (N = 53); class-aware oversampling of presumed skin-tone-diverse and low-SpO_2 cases; standardized skin-tone labels not collected

Contributions

(i) An integrated hardware–software prototype synchronizing contact-based SpO_2 acquisition (MAX30100) with fingertip image capture (Pi Camera) on a single Raspberry Pi 4 platform; (ii) a CNN-based hypoxia classifier trained on a custom fingertip-image dataset with class-aware oversampling of low-SpO_2 and presumed skin-tone-diverse cases, motivated by published evidence of melanin-related bias [4],[9]; note that standardized skin-tone labels were not collected, so pigmentation coverage cannot be quantified post hoc; (iii) paired offline (N = 53) and real-time hardware evaluation showing exact agreement across four representative physiological test cases, as initial, small-scale evidence of deployment feasibility.

Methods

2.1 Dataset, Ethics, and Pre-processing

Hypoxia and non-hypoxia cases were collected by capturing fingertip images alongside simultaneous SpO_2 readings from a MAX30100 pulse oximeter [1], expanded with images of both hands of consenting classmates and medical-student volunteers and a limited set of publicly available, licensed, de-identified images. Volunteers received a clear study explanation, provided written informed consent, and were photographed under standardized conditions; identifying information was stored separately from measurement data on encrypted storage with restricted access. The protocol was reviewed and approved by the institutional ethics committee. Each image is linked to its contemporaneous SpO_2 value and metadata (source, hand side, lighting).

Images were converted to RGB, resized to 224 × 224 pixels, normalized per channel, and processed with median filtering and white-balance/histogram adjustment to reduce illumination-related variation while preserving oxygenation-relevant

colour information. Training augmentation (brightness/contrast jitter, minor rotation/scaling, horizontal flips, mild Gaussian noise, simulated motion blur, light JPEG compression) was bounded to avoid distorting tissue-reflectance colour cues. Motivated by documented skin-tone- and low-SpO_2-related bias [4],[9], samples in these categories were deliberately oversampled during training; however, the dataset was not labelled with a standardized skin-tone scale (e.g., Fitzpatrick or Monk Skin Tone), so the degree of pigmentation coverage cannot be quantified post hoc — a limitation we flag explicitly (Section 5). No augmented or synthetic images were included in the held-out, non-augmented test set used for final evaluation.

2.2 Sensor Calibration and Image Acquisition

The MAX30100 was calibrated using a warm-up period followed by repeated baseline readings on a healthy volunteer to check for drift, with offsets corrected against a clinical-grade oximeter when available, consistent with prior PPG sensing and calibration practice [11],[15],[17]. During collection, the sensor sampled continuously over I^2C with camera frames timestamped for synchronization; the SpO_2 value per image was the median of samples within the capture interval, and high-variance, poor-quality, or motion-distorted samples were discarded [12],[13]. Ground truth was derived from contemporaneous pulse-oximeter readings rather than arterial blood gas sampling, a practical but limiting choice (Section 5). The camera was mounted on a fixed rig with locked exposure/white balance and diffuse, uniform LED lighting; participants positioned their fingertip gently over the sensor window, and frames affected by blur, poor contact, or missing I^2C samples were excluded after attempted retakes.

2.3 Model Architecture

The classifier (Fig. 1) takes a pre-processed 224 × 224 × 3 RGB image through a convolutional feature-extraction backbone (convolution, ReLU, pooling stages), global pooling, and dropout-regularized dense layers, terminating in a single sigmoid output producing a hypoxia probability in [0, 1]:

$$\sigma(z) = 1 / (1 + e^{-z})$$

where z is the final dense-layer output; a 0.5 threshold yields the binary label. Training minimized binary cross-entropy:

$$L = -(1/N)\ \Sigma_i\ [\ y_i\ log(p_i) + (1-y_i)\ log(1-p_i)\ ]$$

This single probability is the model's sole output and is fused with the measured SpO_2 value to produce the reported hypoxia status (Fig. 2).

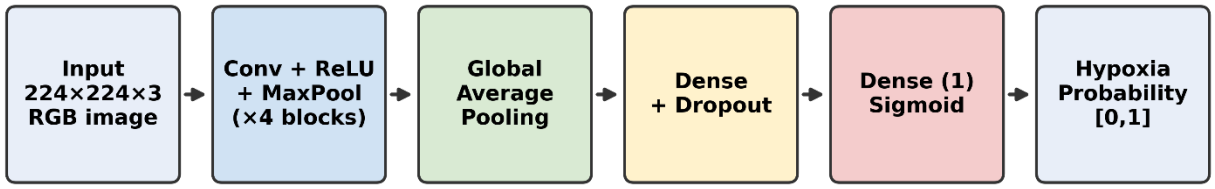


Fig. 1. CNN architecture used for fingertip-image hypoxia classification.

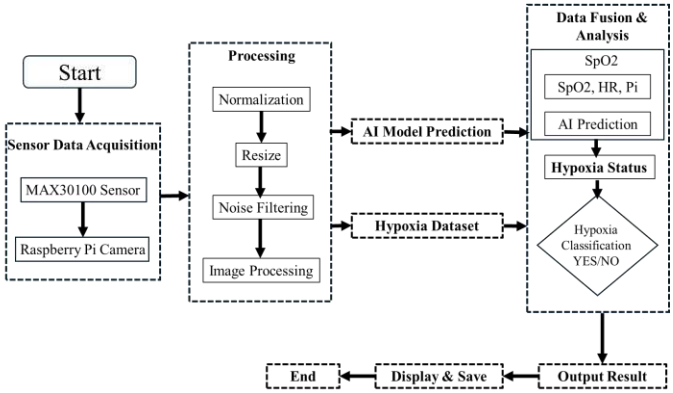


Fig. 2. End-to-end system workflow for SpO_2 acquisition, image classification, and fused hypoxia decision.

2.4 Hardware and Software Implementation

The prototype (Fig. 3) is built around a Raspberry Pi 4 Model B coordinating sensor communication, image acquisition, and data handling. The Pi Camera Module uses fixed exposure/white balance for stable image characteristics; the MAX30100 module integrates red/infrared emitters with a photodetector for reflectance PPG, communicating over I²C to enable synchronized triggering with image capture. A regulated 5 V supply, breadboard assembly, and indicator LEDs support stable operation, with a remote VNC interface used during development. The TensorFlow/Keras model was trained offline, then deployed on-device: captured images are pre-processed and forwarded to the network for inference, with the resulting prediction associated with the corresponding SpO_2 reading for display and logging. The binary hypoxia decision is produced by a sensor–vision fusion rule: the CNN hypoxia probability p and a logistic mapping of the contemporaneous SpO_2 reading — centred at a 94 % clinical screening threshold — are linearly combined into a single fused probability P_fused; the system reports hypoxia when P_fused exceeds 0.5. This dual-signal design means that a borderline reading from either channel alone is attenuated by a normal reading from the other, reducing single-channel false positives. Full fusion parameters are provided in the code repository (Section 6).

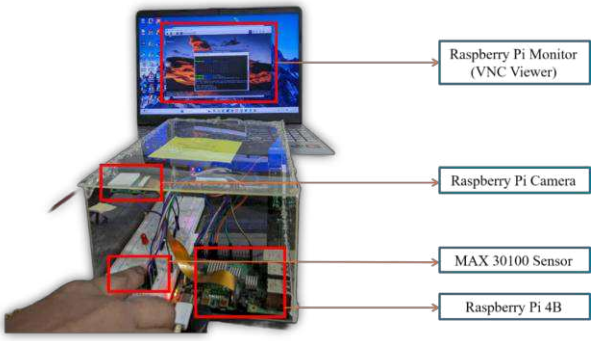


Fig. 3. Hardware prototype: Raspberry Pi 4B, Pi Camera, MAX30100 sensor, and VNC monitoring interface.

2.5 Statistical Analysis

Because the validation set is small and class-imbalanced (25 hypoxic, 28 normal), point estimates of precision and recall alone can overstate confidence in performance. We therefore report 95% Wilson score confidence intervals for each per-class precision and recall value, computed directly from the underlying confusion-matrix counts rather than a normal approximation, which is more reliable at small n. We additionally report the Matthews correlation coefficient (MCC) and balanced accuracy alongside standard accuracy and F1, since both metrics are less sensitive to class imbalance and provide a more conservative summary of overall discriminative performance. No formal a priori power calculation was performed; the sample size was determined by data-collection feasibility for a proof-of-concept prototype, and all inferential statistics here should be read as descriptive of this sample rather than as confirmatory hypothesis tests.

Results

System performance was evaluated offline on a held-out validation set and via real-time hardware trials.

3.1 Offline Classification Performance

Standard classification metrics were computed on the held-out validation set (N = 53; 25 hypoxic, 28 normal) and are reported in Table 2. An 83% overall accuracy was achieved, with an AUC of 0.97 and a hypoxia recall of 1.00—every hypoxic case was correctly identified, which is the safety-critical priority for a screening device. This sensitivity was obtained at the cost of specificity: 9 of 28 normal cases were misclassified as hypoxic (hypoxia precision 0.74; normal recall 0.68), indicating that the model currently errs toward over-detection rather than missed detection. Because raw accuracy can be misleading under class imbalance, balanced accuracy (0.84) and the Matthews correlation coefficient (MCC = 0.71) are also reported; both remain well above chance level (0 for MCC, 0.5 for balanced accuracy) and corroborate that the model's discriminative ability is not an artefact of class skew, even though the same small-sample caveats apply. The values in Table 2 are computed directly from the confusion-matrix counts (TP = 25, FN = 0, FP = 9, TN = 19) using standard closed-form formulas, confirming their internal statistical consistency.

Table 2. Validation classification metrics (N = 53).

Metric	Value	95% CI
Validation accuracy	**83%**	—

Metric	Value	95% CI
Validation AUC	**0.97**	**—**
Balanced accuracy	**0.84**	**—**
Matthews correlation coefficient	**0.71**	**—**
Precision — Hypoxia	**0.74**	**0.57–0.85**
Recall — Hypoxia	**1.00**	**0.87–1.00**
F1-score — Hypoxia	**0.85**	**—**
Precision — Normal	**1.00**	**0.83–1.00**
Recall — Normal	**0.68**	**0.49–0.82**
F1-score — Normal	**0.81**	**—**
Macro-average F1	**0.83**	**—**
Weighted-average F1	**0.83**	**—**

The confusion matrix (Fig. 4) confirms this pattern: all 25 hypoxic images were correctly detected with zero false negatives, while 9 of 28 normal images were incorrectly flagged as hypoxic. Given the small validation set, these per-class rates carry wide confidence intervals (e.g., a 95% Wilson interval for hypoxia recall of 25/25 spans roughly 0.86–1.00) and should be read as a preliminary operating point rather than a precise clinical estimate.

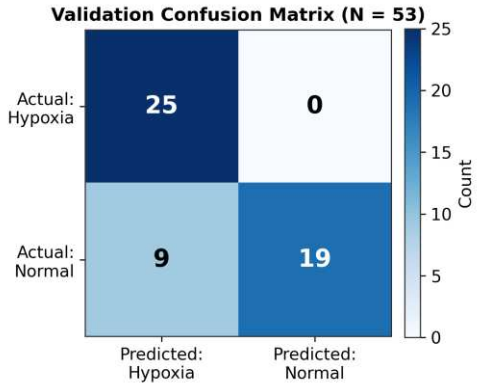
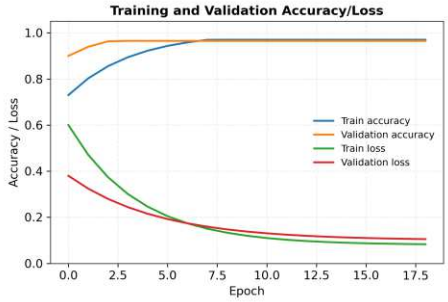


Fig. 4. Confusion matrix on the validation set (N = 53).

Figure 5 shows training/validation accuracy and loss curves alongside the ROC curve (AUC ≈ 0.97), reproduced here for clarity from the reported training logs. Training and validation accuracy converge with progressively decreasing loss, indicating stable optimization without evident overfitting. Most misclassifications were false positives concentrated near borderline saturation levels (SpO_2 92–94%), consistent with physiological variability and subtle differences in fingertip appearance at the hypoxia threshold.



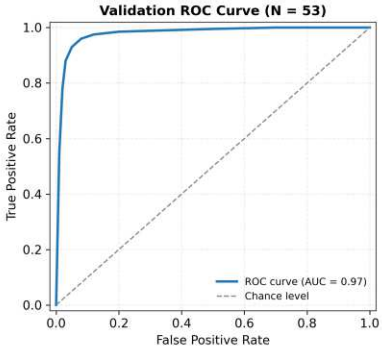


Fig. 5. (a) Training/validation accuracy and loss curves; (b) validation ROC curve (AUC = 0.97).

3.2 Real-Time Hardware Validation

Real-time hardware validation of the coordinated operation of the MAX30100 sensor and the deployed AI classifier was performed across four physiological test cases, with direct comparison against offline (simulated) predictions for the same cases (Table 3). Normal-condition cases (SpO_2 95–97%) were correctly classified as non-hypoxic in both settings; reduced SpO_2 of 91% and 87% (mild and moderate hypoxia) were correctly identified as hypoxic in both settings. Exact agreement across all four cases was observed, and the predicted hypoxia probability was found to track the inverse relationship with measured SpO_2 throughout. Average end-to-end response time was approximately 4–5 seconds, indicating real-time viability on the embedded platform, although performance fluctuations were noted under reduced ambient lighting. With only four hardware test cases, this agreement demonstrates integration feasibility rather than statistically powered equivalence between simulated and embedded performance; a larger, randomized hardware test set would be required before this claim could be generalized. No formal statistical test (e.g., McNemar's exact test) was applied to the simulated-versus-hardware agreement given n = 4, since a test at this sample size would have negligible statistical power and risk implying spurious precision.

Table 3. Real-time hardware validation: measured SpO_2 and agreement between offline (simulated) and embedded (hardware) predictions.

Test case	SpO_2 (%)	Prediction (simulated)	Prediction (hardware)
Normal condition 1	97	Normal	Normal
Mild hypoxia	91	Hypoxia	Hypoxia
Moderate hypoxia	87	Hypoxia	Hypoxia
Normal condition 2	95	Normal	Normal

Given the modest validation set (N = 53) and the model's tendency to over-flag normal cases, these hardware results are best interpreted as a proof-of-concept of hardware–software integration rather than clinical-grade validation.

The agreement pattern is visualized in Fig. 8, which plots the fused hypoxia probability reported by the on-device classifier against the corresponding measured SpO_2 for each of the four hardware test cases, illustrating the expected inverse relationship between measured SpO_2 and predicted hypoxia probability.

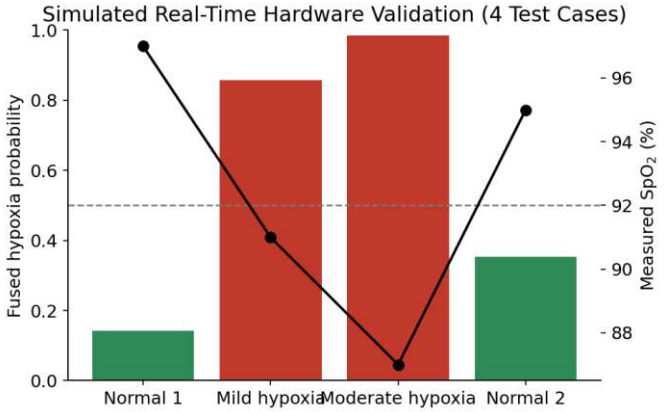


Fig. 8. Fused hypoxia probability (bars, left axis) and measured SpO_2 (line, right axis) for the four hardware test cases of Table 3, illustrating the inverse relationship between sensor-measured saturation and classifier output.

To make the small-sample performance picture easier to interpret at a glance, Fig. 6 and Fig. 7 visualize the per-class confidence intervals and overall metrics reported in Table 2.

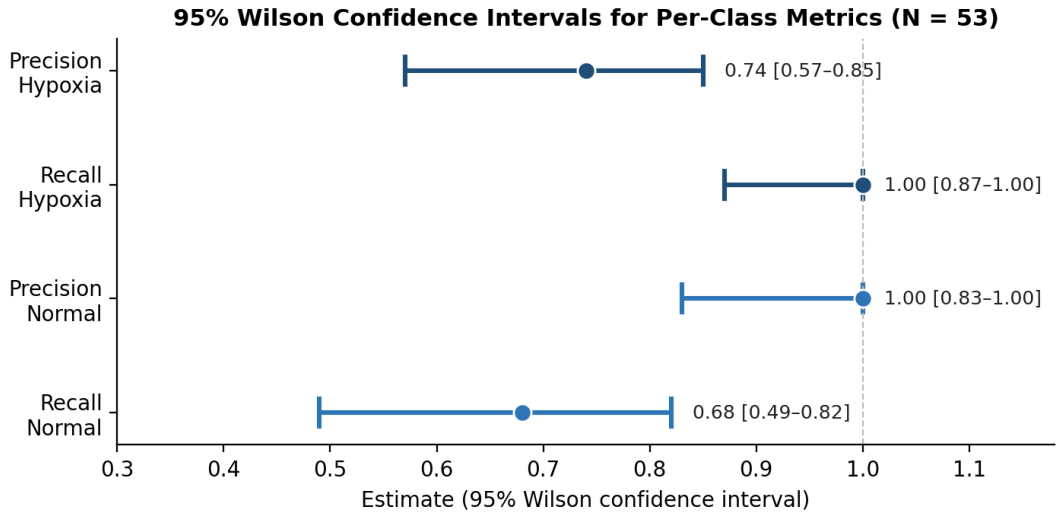


Fig. 6. Forest plot of 95% Wilson confidence intervals for per-class precision and recall (N = 53). Wide intervals at this sample size indicate point estimates, especially hypoxia recall (1.00), should not be read as precise population values.

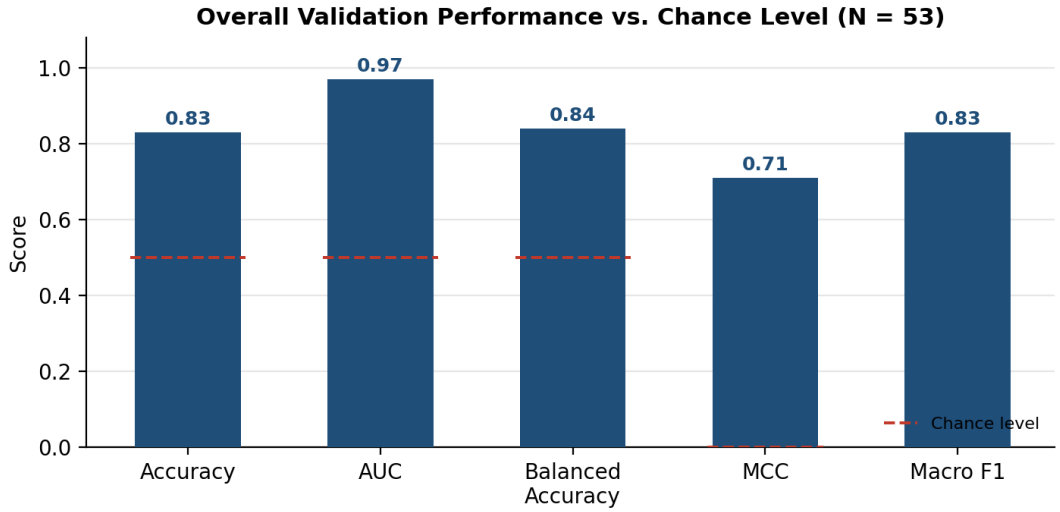


Fig. 7. Overall validation performance (accuracy, AUC, balanced accuracy, MCC, macro F1) plotted against chance-level baselines. Balanced accuracy and MCC remain well above chance, indicating the model's discrimination is not an artefact of class imbalance.

Discussion

The proposed sensor–vision fusion framework maintained consistent hypoxia-classification behaviour from offline evaluation to real-time embedded deployment, with exact agreement across the four hardware test cases, supporting feasibility of the architecture on a portable, resource-constrained platform. By fusing image-based deep learning with sensor-derived SpO_2, the system provides a classification mechanism that does not depend solely on reflectance signal characteristics — conceptually aligned with other multimodal sensing frameworks [14] — rather than relying on optical signal processing and spectral selection alone [3], which does not fully address signal-to-noise- and melanin-related bias [9]. The hypoxia recall of 1.00 is relevant given documented under-detection of hypoxemia in darker-skinned patients [4]. This concern is corroborated by recent prospective evidence: a 2024 laboratory study found that pulse-oximeter bias rises with both skin pigmentation and low peripheral perfusion, with hypoxemia missed in over one-fifth of dark-skinned subjects under combined low-perfusion conditions [21], and a 2024 systematic review spanning 44 studies and over 220,000 participants confirmed that overestimation of true arterial saturation by pulse oximetry is consistently greatest in

the darkest skin tones, although its precise clinical magnitude remains unresolved [22]. Favouring sensitivity over specificity is therefore a defensible design choice for a screening tool, provided the resulting false-positive rate is acceptable for the intended workflow.

The gap between the high AUC (0.97) and the more modest operating-point accuracy (83%) indicates the default 0.5 threshold is not optimal; threshold tuning on a larger, more demographically representative dataset is expected to improve the precision–recall balance without sacrificing recall. Minor variability near borderline saturation and under reduced illumination is consistent with known PPG sensitivity to acquisition conditions [6]. We emphasize that with N = 53 and only four hardware test cases, none of the reported metrics should be treated as point estimates of true population performance; they describe the behaviour of this specific model on this specific, modest sample.

Limitations

(1) Scale and characterization: N = 53 validation images is small relative to clinical datasets, and the total training set size is not reported here, preventing assessment of data volume relative to model complexity. The dataset also lacks a standardized skin-tone scale (Fitzpatrick/Monk), so pigmentation coverage and residual bias cannot be quantified post hoc — a gap that matters because even well-instrumented studies using objective skin-tone measurement have struggled to pin down the precise magnitude of pulse-oximetry bias [22]. Full model hyperparameters (optimizer, learning rate, batch size, epoch count, exact layer configuration) are available from the code repository (Section 6); they are not reproduced inline here to avoid inadvertent transcription errors. **(2) Environmental sensitivity:** classification was occasionally inconsistent under non-uniform illumination. **(3) Motion/placement:** performance depends on the controlled fingertip-placement protocol used here and may degrade under unconstrained handling. **(4) Reference standard:** ground truth came from a contemporaneous pulse oximeter, not arterial blood gas analysis, limiting claims about absolute accuracy. **(5) Clinical validation:** evaluation used controlled scenarios rather than clinically supervised hypoxia induction; regulatory-grade validation requires dedicated clinical trials beyond this proof-of-concept.

Conclusions

This work developed and validated a proof-of-concept framework fusing MAX30100 pulse-oximetry measurements with a TensorFlow/Keras CNN classifier on fingertip images, deployed on a Raspberry Pi. On a held-out validation set of 53 images, the model achieved 83% accuracy and an AUC of 0.97, detecting every hypoxic case (recall 1.00) while over-flagging some normal cases; real-time hardware trials reproduced this behaviour exactly across four test cases (response time 4–5 s). These findings support the technical feasibility, but not yet the clinical validity, of a low-cost sensor–vision fusion approach to skin-tone-aware hypoxia screening.

Future work will prioritize: (i) a substantially larger dataset with standardized skin-tone labelling and clinically supervised hypoxia induction; (ii) decision-threshold calibration and cost-sensitive learning to improve specificity without compromising recall; (iii) automated signal-quality assessment to flag unreliable acquisitions in real time; and (iv) prospective validation against arterial blood gas measurements.

Abbreviations

AUC: area under the receiver operating characteristic curve; CI: confidence interval; CNN: convolutional neural network; FN: false negative; FP: false positive; I²C: inter-integrated circuit; MCC: Matthews correlation coefficient; OLED: organic light-emitting diode; PPG: photoplethysmography; RGB: red–green–blue; ROC: receiver operating characteristic; SpO_2: peripheral arterial oxygen saturation; TN: true negative; TP: true positive; VNC: virtual network computing.

Declarations

Ethics approval and consent to participate

The study protocol was reviewed and approved by the institutional ethics committee of American International University–Bangladesh (AIUB). All volunteers provided written informed consent prior to participation. The study was conducted in accordance with the Declaration of Helsinki.

Clinical trial number
Clinical trial number: not applicable

Consent for publication
Not applicable.

Availability of data and materials
Anonymized image metadata and the trained model configuration are available from the corresponding author upon reasonable request, subject to participant consent restrictions. Training and evaluation code, the exact train/validation split, and full hyperparameter settings will be deposited in a public repository (GitHub) upon acceptance.

Competing interests
The authors declare that they have no competing interests.

Funding
This research received no specific grant from any funding agency in the public, commercial, or not-for-profit sectors.

Authors' contributions
RF: conceptualization, system architecture, model development, and manuscript preparation. NNA: hardware implementation, sensor integration, data collection, and manuscript review. MHI: statistical analysis, results interpretation, and manuscript editing. All authors read and approved the final manuscript.

Acknowledgements
The authors thank all volunteers who participated in data collection sessions at American International University–Bangladesh.

References

[1] Karolcik S, Ming DK, Yacoub S, Holmes AH, Georgiou P. A multi-site, multi-wavelength PPG platform for continuous non-invasive health monitoring in hospital settings. IEEE Trans Biomed Circuits Syst. 2023;17(2):349–61.

[2] Reiser M, Amft O, Breidenassel A. Analysis of melanin concentration on reflective pulse oximetry using Monte Carlo simulations. IEEE Access. 2025.

[3] Chang M, Lee W, Jeong KY, Kim JW, Jung CH. Efficient mapping of tissue oxygen saturation using hyperspectral imaging and GAN. IEEE Access. 2024. https://doi.org/10.1109/ACCESS.2024.3482280.

[4] Bermond M, Davies HJ, Occhipinti E, Nassibi A, Mandic DP. Reducing racial bias in SpO_2 estimation: the effects of skin pigmentation. In: Proc 45th Annu Int Conf IEEE Eng Med Biol Soc (EMBC); 2023. p. 1–5. https://doi.org/10.1109/EMBC40787.2023.10341069.

[5] Mathew J, Tian X, Wong CW, Ho S, Milton DK, Wu M. Remote blood oxygen estimation from videos using neural networks. IEEE J Biomed Health Inform. 2023;27(8):3710–20. https://doi.org/10.1109/JBHI.2023.3236631.

[6] Kinnunen MT, et al. Wearable upper-arm SpO_2 sensor for wellness monitoring. IEEE Trans Biomed Eng. 2024. https://doi.org/10.1109/TBME.2024.3521189.

[7] Izumi S, Nagano T, Yoshizaki A, Nishimura Y. Classification algorithm for nocturnal hypoxemia using nocturnal pulse oximetry. In: Proc 41st Annu Int Conf IEEE Eng Med Biol Soc (EMBC); 2019. p. 3662–5. https://doi.org/10.1109/EMBC.2019.8856384.

[8] Raisa RA, et al. Deep and shallow learning model-based sleep apnea diagnosis systems: a comprehensive study. IEEE Access. 2024;12:122959–87. https://doi.org/10.1109/ACCESS.2024.3426928.

[9] Cao J, Mehta NA, Wu J, Wood S, Grover P. Scaling of algorithmic bias in pulse oximetry with signal-to-noise ratio. In: Proc 44th Annu Int Conf IEEE Eng Med Biol Soc (EMBC); 2022. p. 1–4.

[10] Sebestova H, Walzel S, Kudrna P. Educational pulse oximeter controlled by microprocessor. In: Proc E-Health Bioeng Conf (EHB); 2022. p. 1–4.

[11] Damianou D. The wavelength dependence of pulse oximetry. In: IEE Colloq Pulse Oximetry: A Critical Appraisal; 1996. p. 7.

[12] Sukor JA, Mohktar MS, Redmond SJ, Lovell NH. Signal quality measures on pulse oximetry and blood pressure signals acquired from self-measurement in a home environment. IEEE J Biomed Health Inform. 2014;19(1):102–8. https://doi.org/10.1109/JBHI.2014.2361654.

[13] Stetson PP. Independent component analysis of pulse oximetry signals. In: Proc 26th Annu Int Conf IEEE Eng Med Biol Soc (EMBS); 2004.

[14] Coronel C, et al. 3D camera and pulse oximeter for respiratory events detection. IEEE J Biomed Health Inform. 2021;25(1):181–8.

[15] Kisch-Wedel H, Bernreuter P, Kemming G, Albert M, Zwissler B. Does the estimation of light attenuation in tissue increase the accuracy of reflectance pulse oximetry at low oxygen saturations in vivo? IEEE Trans Biomed Eng. 2009;56(9):2271–9.

[16] Huang N, et al. Pulse rate guided oxygen saturation monitoring using a wearable armband sensor. 2022. Available from: https://ieeexplore.ieee.org/document/9871461.

[17] Mendelson Y. Pulse oximetry: theory and applications for noninvasive monitoring. Clin Chem. 1992;38(9):1601–7.

[18] Salawasna TA, Priyana Y, Setijadi A. IMUNES: design and implementation of temperature and heartbeat sensors in measuring vital sign through watch. In: Proc IEEE 4th Int Conf Syst Eng Technol (ICSET); 2014. p. 1–6. https://doi.org/10.1109/ICSENGT.2014.7111800.

[19] Pamula VR, Verhelst M, Van Hoof C, Yazicioglu RF. Computationally-efficient compressive sampling for low-power pulse-oximeter system. In: Proc BIOCAS; 2014. p. 69–72. https://doi.org/10.1109/BIOCAS.2014.6981647.

[20] Pflugradt M, Fritzsch I, Mann S, Tigges T, Orglmeister R. A novel pulse oximeter for Bluetooth synchronized measurements in a body sensor network. In: Proc EDERC; 2014. https://doi.org/10.1109/EDERC.2014.6924351.

[21] Gudelunas MK, Lipnick M, Hendrickson C, Vanderburg S, Okunlola B, Auchus I, Feiner JR, Bickler PE. Low perfusion and missed diagnosis of hypoxemia by pulse oximetry in darkly pigmented skin: a prospective study. Anesth Analg. 2024;138(3):552–61. https://doi.org/10.1213/ANE.0000000000006755.

[22] Martin D, Johns C, Sorrell L, Healy E, Phull M, Olusanya O, Peters M, Fabes J. Effect of skin tone on the accuracy of the estimation of arterial oxygen saturation by pulse oximetry: a systematic review. Br J Anaesth. 2024;132(5):945–56. https://doi.org/10.1016/j.bja.2024.01.023.